Navigation of Frameless Fixation for Gammaknife Radiosurgery Using Fixed Augmented Reality

Hyeong Cheol Moon
Chungbuk National University Hospital
Sang Joon Park
MEDICALIP Co. Ltd
Youngdeok Kim
MEDICALIP Co. Ltd
Kyung Min Kim
Seoul National University Hospital, Seoul National University College of Medicine
Ho Kang
Seoul National University Hospital, Seoul National University College of Medicine
Eun Jung Lee
Seoul National University Hospital, Seoul National University College of Medicine
Min-Sung Kim
Seoul National University Hospital, Seoul National University College of Medicine
Jin Wook Kim
Seoul National University Hospital, Seoul National University College of Medicine
Yong Hwy Kim
Seoul National University Hospital, Seoul National University College of Medicine
Chul-Kee Park
Seoul National University Hospital, Seoul National University College of Medicine
Young Gyu Kim
Chungbuk National University Hospital, Chungbuk National University College of Medicine
Yun-Sik Dho (ysdho@chungbuk.ac.kr)
Chungbuk National University Hospital, Chungbuk National University College of Medicine

Research Article

Keywords: 3D-scanning, cone beam computed tomography scanning, frameless fixation navigation, fixed augmented reality, gammaknife radiosurgery.

Posted Date: September 15th, 2021

DOI: https://doi.org/10.21203/rs.3.rs-879840/v1

Abstract

Augmented reality (AR) offers a new medical treatment approach. We aimed to evaluate frameless fixation navigation using a 3D-printed patient model with fixed-AR technology for gammaknife radiosurgery. Fixed-AR navigation was developed using the inside-out method with visual inertial odometry algorithms, and the flexible Quick Response (QR) marker was created for object-feature recognition. Virtual 3D-patient models for AR-rendering were created *via* 3D-scanning utilizing TrueDepth and cone-beam computed tomography (CBCT) to generate a new GammaKnife Icon™ model. A 3D-printed patient model included fiducial markers, and virtual 3D-patient models were used to validate registration accuracy. Registration accuracy between initial frameless fixation and re-fixation navigated fixed-AR was validated through visualization. The quantitative method was validated through set-up errors, fiducial marker coordinates, and high-definition motion management (HDMM) values. 3D-printed models and virtual models were correctly overlapped under frameless fixation. Virtual models from both 3D-scanning and CBCT were enough to tolerate the navigated frameless re-fixation. Although the CBCT virtual model consistently delivered more accurate results, 3D-scanning was sufficient. Frameless re-fixation accuracy navigated in virtual models had mean set-up errors within 1 mm and 1.5° in all axes. Mean fiducial marker differences from coordinates in virtual models were within 2.5 mm in all axes, and mean 3D errors were within 3 mm. Mean HDMM difference values in virtual models were within 1.5 mm of initial HDMM values. The variability from navigation fixed-AR is enough to consider repositioning frameless fixation without CBCT scanning for treating patients fractionated with large multiple metastases lesions (>3 cm) who have difficulty enduring long beam-on time. This system could be applied to novel radiosurgery navigation for frameless fixation with reduced preparation time.

Introduction

Augmented reality (AR) is an advanced technology that mixes the virtual world with the real world in different proportions[30]. It has found good potential applications in many fields, such as military training, entertainment, manufacturing, and medical, in recent years. In the neurosurgery field, AR is used as a volumetric image guide[23,26] and phone-based neurosurgical navigation system[7,8,20]. AR navigation uses various devices such as smartphones, desktop PCs, head-mounted displays, and AR glasses. The AR system commonly consists of an outside-in method using sensors either attached to the computer, head-mounted display, or pre-installed, which can be operated intuitively in conjunction with hand movements[10], but sensor recognition could go out-of-range due to misalignment after initial registration. The inside-out tracking method can detect a continuous tracing of the target from the user's location through cameras and sensors mounted simultaneously on the device used for visualization[16]. Although inside-out tracking has less accuracy compared to outside-in tracking, installing the equipment for visualization and object detection for registration is low cost. We previously reported on an inside-out tracking-based AR-neuro-navigation system using ARKit®-based software (Apple Inc., CA, USA)[5]. We applied the inside-out tracking for radiosurgery by mounting it to an iPad® (Apple Inc., CA, USA) to test the feasibility to develop clinically usable inside-out tracking AR in gammaknife radiosurgery (GKRS), which utilizes devices in a fixed-stated, called fixed-AR.

The high dose of radiation delivered through GKRS requires a high degree of accuracy and immobilization of the head[3,14]. Accuracy with head-frame fixation is essential to limit irradiation of the surrounding anatomical structures[15]. Head-frame placement is invasive involving screw fixation at four specific points in the patient's skull and difficult for fractionated treatment of large lesions[3,19]. The latest version in GammaKnife Icon is capable of non-invasive fixation and fractionated treatment by utilizing cone-beam computed tomography (CBCT) and detecting the motion by high-definition motion monitoring (HDMM). CBCT could be acquired by either a higher signal (CTDI 6.3) present or lower dose (CTDI 2.5) and registered with the stereotactically-defined image set for comparison between patient coordinates at the time of treatment imaging; the HDMM system can currently be used for head immobilization with a thermoplastic mask

instead of a head-frame[6]. During subsequent delivery of the adapted treatment plan from the HDMM system, it tracks the displacement of the patient's nose marker related to the four immobile reflectors fixed to the Icon™ head support system in real time[27]. However, the irradiation is executed only when the magnitude of displacement returns under the threshold; if the threshold is exceeded, the new CBCT scan is processed to allow coordinates acquire a new position. Wright et al. suggested that the target and nose marker typically varies throughout a clinically relevant extent of stereotactic space, and the average HDMM threshold of 1.4 mm may have been appreciated for 41 volumes[27]. However, patients with multiple metastases or older age seem to be intolerant to the lower threshold according to the increased beam-on time. Kim et al. reported that the elapsed beam-on time, including beam-paused time due to motion of the patient, defines the tolerance for around 30 minutes (min) in older patients (> 65 years)[9]. Thus, keeping the appropriate HDMM threshold without the new position for CBCT scanning is important for intolerant patients in GKRS frameless fixation. The navigation of patient positioning under frameless fixation is useful to reduce the preparation time and unnecessary CBCT scanning. If we used CBCT images to make a 3-dimensional (3D)-virtual model using fixed-AR, the frameless fixation could possibly be repositioned, guided by a 3D-virtual model, based on initial planning for CBCT without unnecessary CBCT scanning.

3D-scanning increases the accuracy and makes it easy to obtain the virtual 3D-model. Recently, TrueDepth technology in the latest devices by Apple Inc. is used for measuring the task with accuracies in the millimeter range. TrueDepth uses vertical-cavity surface-emitting laser (VCSEL) technology and consists of an infrared camera, a conventional camera, proximity sensor, pot projector, and flood illuminator[25]. The front-facing camera provides the depth data in real-time along with visual information, and the system uses a light-emitting diode to project an irregular grid of over 30,000 infrared dots to record the depth within milliseconds. To scan objects, an additional application was installed[24]. Although Heges application was evaluated with the finest 3D resolutions under 0.5 mm[25], the accuracy is affected by the scanning strategy and post-processing[17]. The potential of TrueDepth in the recent iPad® as 3D-scanning in Heges application was evaluated using fixed-AR in GKRS.

To apply this new AR technology for stereotactic radiosurgery, the virtual models were established using existing planning CBCT images, and a novel TrueDepth 3D-scanning method. In this study, we investigated the navigation of frameless fixation using fixed-AR with the virtual models of CBCT scans and 3D-scans into a 3D-printed patient model for GKRS.

Methods

3D-printed patient model and initial frameless fixation

The 3D-printed patient model was produced in the following three stages: 1) creation of a stereolithography (STL) file for 3D printing; 2) printing physibles using a 3D printer; and 3) post-processing performed *via* manual editing. The process was approved by the institutional review board (Seoul National University Hospital IRB No. 1811-040-96 and Chungbuk National University Hospital, IRB No. 2019-06-015) and used to validate set-up errors, fiducial marker coordinates, and HDMM values. The 3D-printed patient model had a frameless adapter with head cushion and was fixed with a thermoplastic nano mask (Elekta instrument AB, Stockholm, Sweden). In the fixed-AR setting, we measured the initial fiducial marker coordinates after planning CBCT and HDMM, which keep the motion value for 10 min, as shown in Figure 2.

3D scanning and planning CBCT

The 3D-printed patient model with frameless fixation was taken for TrueDepth scanning using Heges application with iPadPro 13 cameras (Apple Inc., One Apple Park Way Cupertino, CA 95014, USA). The .stl scan file of the scan was

imported to Meshmixer version 3.5 (https://www.meshmixer.com) to trim the background scanning, and smoothing processes were performed to improve the pixilation an obtain more uniform triangles.

The 3D-printed patient model with frameless fixation was also taken for planning CBCT scanning using Leksell GammaPlan Version 11.1 (Elekta instrument AB, Stockholm, Sweden), and exported to CBCT dicom files. The dicom files were imported to MEDIP software (MedicalIP, Seoul, Republic of Korea) for 3D-rendering, trimming the background, and smoothing processing. This procedure is shown in Figure 3.

Inside-out AR navigation and running fixed-AR

The inside-out AR navigation was developed by AR framework using ARkit®. The inside-out AR navigation was processed in three steps. First, device recognition is visualized, followed by QR marker recognition, and AR implementation and registration within the running environment. The QR marker is attached to the right mask fixation button adjacent to the matching target that has minimal light reflection and is unlikely to be easily obscured by other objects. The ARkit is based on Visual Inertial Odometry (VIO), which measures the device location from inertial measurement unit (IMU)-based data that has a fast collection and calibrates using camera images. Moreover, ARkit supports close-loop processing that corrects the trajectory by matching the trajectory with the starting point when moving the device and returning to the starting point during calculation with the VIO algorithms. This is collectively referred to as visual inertial simultaneous localization and mapping. The loop-closure process can be omitted due to the nature of this AR system wherein the device operates in a fixed state.

The QR marker images are used for estimating the position recognized by the camera in the feature detection algorithm, which commonly considers the corner and intersection of lines or the part with clear color contrasts (Black and White) as a feature point. After the device position is determined, the QR marker, recognized by the scale of objects in virtual space, is determined by calculating the distance between the device and the QR marker from the size of the recognized marker in the preceding step. After all the requisite data are calculated, the 3D scanning or CBCT-based virtual models are displayed at the designated positions from the marker for confirmation by the user. In case of errors in the automatically processed pre-registration, the user can correct the registration error by adjusting the position of the 3D virtual model using the fine-tuning function and then fix the position of the models to complete the registration.

Validating the fixed-AR navigation registration

The registration accuracy was measured using the following three methods: intuitive validation through visualization; set-up errors; and quantitative validation. The 3D-printed patient model was created and matched with 3D virtual models. Set-up errors were assessed by comparing the planning and pretreatment CBCTs[3], which navigated to re-fixation using fixed-AR system in the virtual models. Set-up errors were investigated by translational (mm) and rotation (°) methods. The registration accuracy of initial fiducial marker was validated by comparing planning CBCT to pretreatment CBCT, which navigated re-fixation in fixed-AR through the virtual models. The fiducial markers were attached to both hemispheres of the 3D-printed patient model in eight points.

We defined the error of coordinates as follows:[11]

Δx=x coordinate in planning CBCT + pretreatment CBCT or virtual models

Δy=y coordinate in planning CBCT + pretreatment CBCT or virtual models

Δz=z coordinate in planning CBCT + pretreatment CBCT or virtual models

Furthermore, the 3D error (Δr) was defined as a localization error by the following formula:

$\Delta r=\sqrt{(\Delta x^2+\Delta y^2+\Delta z^2)}$.

The differences of HDMM values were investigated to initial fixation and re-fixation navigated fixed-AR in the virtual models. The mean accuracy was evaluated by measuring the X, Y, and Z coordinates for the three measurements.

The function of fixed-AR

For cases when automatic registration using the QR marker could be misaligned, the processing is discussed in detail. A fine-tuning function of adjusting the position of the virtual 3D model of AR navigation was developed. The virtual space is seen on the device screen through the following local coordinates, which defined the model orientation. Opacity-adjustment function can be adjusted by using opacity-adjustment function. These functions allow AR implementation by further co-registration in the brain.

Results

Execution of fixed-AR navigation in frameless fixation

When the navigation of frameless fixation is executed through the new application, it is overlapped on the 3D-printed model. To complement the fixed device state, the quick response (QR) marker attached to the mask indicator and iPad is stalled to the cradle beside a couch bed. The QR marker was designed for various directions by adjusting the registration target. Fixed-AR navigation could be seen to correctly overlap with the 3D-printed patient model and virtual models based on 3D-scanning and CBCT in Fig. 1.

Validation of frameless fixation based on virtual models using Fixed-AR

Rotational and translational set-up errors for frameless fixation based on virtual models using fixed-AR are summarized in Table 1. The mean rotational errors for the virtual models were small in all axes, less than 1.0° except for the Y-axis (1.36 ± 1.064°) in the 3D-scanning virtual model. The mean translation error for the virtual models was less than 1 mm in all axes.

Table 1
The mean translational and rotational set-up errors in frameless fixation using fixed-AR

	Planning CBCT + pretreatment CBCT	**Planning CBCT + Virtual model of 3D-scanning with fixed-AR**	**Planning CBCT + Virtual model of CBCT with fixed-AR**
Rotation (°)			
x-axis	0.010 ± 0.010	0.313 ± 0.364	0.387 ± 0.523
y-axis	0.007 ± 0.012	1.360 ± 1.064	0.880 ± 1.060
z-axis	0.013 ± 0.06	0.743 ± 0.801	0.587 ± 0.611
Translational (mm)			
x-axis	0.027 ± 0.029	0.403 ± 0.038	0.677 ± 0.422
y-axis	0.040 ± 0.010	0.190 ± 0.135	0.297 ± 0.249
z-axis	0.013 ± 0.015	0.633 ± 0.215	0.820 ± 0.887
All data are shown as mean ± standard deviation.			

The fiducial markers in the 3D-printed model are defined in seven points out of eight points because of the exceeding image definition from CBCT scanning. The mean error of fiducial marker coordinates for frameless fixation based on virtual models using fixed-AR are summarized in Table 2. Comparison of the planning CBCT with pretreatment CBCT showed all mean errors were under 1.0 mm. However, the planning CBCT with virtual models had a mean error of 0.75 to 2.72 mm, including 3D errors.

Table 2
The mean errors of fiducial marker coordinates in virtual models with fixed-AR

	Planning CBCT + pretreatment CBCT				**Planning CBCT + Virtual model of 3D-scanning with fixed-AR**				**Planning CBCT + Virtual model of CBCT with fixed-AR**			
Location of fiducial markers	Δx (mm)	Δy (mm)	Δz (mm)	Δr (mm)	Δx (mm)	Δy (mm)	Δz (mm)	Δr (mm)	Δx (mm)	Δy (mm)	Δz (mm)	Δr (mm)
Left frontal	0.48 ± 0.11	0.52 ± 0.17	0.35 ± 0.11	0.90 ± 0.20	1.31 ± 0.85	0.99 ± 0.51	2.15 ± 1.42	2.71 ± 1.75	1.16 ± 1.20	0.71 ± 0.30	1.33 ± 1.48	2.10 ± 1.59
Right frontal	0.29 ± 0.19	0.44 ± 0.19	0.14 ± 0.07	0.75 ± 0.30	1.35 ± 1.11	1.29 ± 0.97	1.77 ± 0.83	2.72 ± 1.34	1.29 ± 1.38	0.95 ± 0.62	1.01 ± 0.98	2.22 ± 1.14
Left parietal	0.44 ± 0.43	0.24 ± 0.14	0.14 ± 0.13	0.68 ± 0.21	0.57 ± 0.50	0.76 ± 0.61	2.32 ± 0.68	2.63 ± 0.43	0.90 ± 1.03	0.94 ± 0.37	2.04 ± 0.40	2.57 ± 0.47
Right parietal	0.29 ± 0.11	0.50 ± 0.41	0.05 ± 0.03	0.59 ± 0.32	0.49 ± 0.29	1.38 ± 0.57	1.73 ± 1.41	2.38 ± 1.26	1.50 ± 0.75	0.82 ± 0.77	1.73 ± 1.18	2.58 ± 1.24
Superior parietal	0.40 ± 0.36	0.50 ± 0.26	0.34 ± 0.27	0.73 ± 0.22	1.85 ± 1.61	0.79 ± 0.73	0.99 ± 0.90	2.72 ± 0.63	1.25 ± 0.77	1.56 ± 0.91	0.84 ± 0.73	2.39 ± 0.71
Inferior parietal	0.45 ± 0.40	0.39 ± 0.05	0.42 ± 0.27	0.78 ± 0.09	1.15 ± 0.14	0.55 ± 0.74	0.78 ± 0.68	1.65 ± 0.53	1.74 ± 1.16	0.85 ± 0.69	1.37 ± 0.57	2.44 ± 1.30
Posterior occipital	0.39 ± 0.33	0.39 ± 0.34	0.26 ± 0.20	0.71 ± 0.19	1.53 ± 0.99	0.54 ± 0.13	0.75 ± 0.54	1.93 ± 0.70	1.23 ± 0.96	0.28 ± 0.29	1.16 ± 0.89	1.92 ± 0.91

All data are shown as mean ± standard deviation.

For patients undergoing GKRS treatment with mask-fixation for a few days, we measured the HDMM differences between initial fixation and re-fixation, navigated by the virtual models for three days. The mean differences in the virtual model of 3D-scanning and CBCT were 1.19 ± 0.32 and 1.21 ± 0.02, respectively. The re-fixation navigated by the virtual models without CBCT showed HDMM values under 1.5 mm.

Optimization of frameless fixation with fine-tunning function

In cases of inaccurate registration after fixed-AR navigation, the user could use the fine-tuning function to adjust the surface position of the fixed-AR navigation that accurately overlaps with the nose marker in GKRS. Both 3D rendering in 3D scanning and CBCT distorted from registration were adjusted to the correct position using the fine-tuning function.

Discussion

GKRS requires an accurate and precise high-dose radiation for a specific target while minimizing the potential radiation toxicity for the surrounding tissue. Recently, the GK Icon version has been shown to be capable of frameless fixation using CBCT, which is used to verify the patient position during set-up prior to irradiation[4]. Frameless fixation is widely used for large lesions with hypofractionated treatment; it is important to endure the tolerance and long beam-on-time, allowing immobilization of the patient's head. If AR navigation using virtual models could replace the patient's head position navigation, maintaining the appropriate HDMM thresholds without repositioning CBCT scanning could be accomplished more easily, reducing the preparation time and reducing the irradiation during CBCT scanning using Fixed-AR for frameless fixation in GKRS. This study represented the mean set-up errors within 1.5°, and 1 mm in both methods. The mean differences of fiducial markers from coordinates were within 2.5 mm, and the 3D errors were within 3 mm in both methods. The mean differences of HDMM values were within 1.5 mm compared to initial HDMM values. The acceptable accuracy errors are debatable in frameless fixation; commonly, within 3 mm differences are acceptable for patients with brain metastases in no eloquent areas. We demonstrated that virtual models with fixed-AR could be applied for intolerant patients with frameless fixation, requiring repeated CBCT scanning to exceed the HDMM.

Patient-specific planning based on individual characteristics and conditions is important for precision treatment in neurosurgery[13,22]. In radiosurgery, all patients have various lesions including malignant or benign tumors, vascular disease, and functional diseases. In our country, demographic projections for older adults have increased, implying a consequent increase in cancer incidence and mortality in this population[29]. Radiosurgery delivered by highly focusing radiation with sharp dose fall-off is theoretically expected to reduce delayed neurotoxicity[28]. Recently, hypofractionated radiosurgery was found to be effective as a single-session radiosurgery with minimal toxicity for large brain metastases (> 10 cm^3)[12,18]. However, the patients with multiple metastases or older age seem to be intolerant to the lower HDMM values according to increased beam-on time. Thus, keeping the appropriate HDMM threshold without a new CBCT scanning position is important for intolerant patients in frameless fixation in GKRS.

The scanning accuracy decides the potential use of 3D scanner applications. The iOS of Apple's smartphones and tablets provides 3D data without the operator's measurement experiences, called TrueDepth Scanner, based on the structure-light principle[1]. TrueDepth-based 3D scanning shows the highest deviations in cylindricity (0.82 mm in average) and roundness (1.17 mm on average)[25]. In another 3D scanning study, Camison et al. demonstrated that the points calculated from a total of 136 distances had an average deviation (mm) of 0.84[2]. Our results showed that translational errors were less than 1.00 mm in all axes in virtual models. However, the rotational error in the Y-axis was higher in the virtual model of 3D-scanning compared to that of CBCT. All fiducial marker errors were under 3 mm without CBCT scanning. These results could be applied to the patients with metastases, long beam-on-time, and no eloquent areas. Paul et al. demonstrated that when using 3 mm as a cut-off there was no effect on local recurrences identified [21].

The novel method of inside-out fixed AR is performed by a physician or physicist experienced in GKRS to match the nose marker target under frameless fixation based on user-determined registration between the 3D-printed patient model and virtual models. Although the fixed-AR images do not execute the automatic registration into frameless fixation, the position of fixed-AR images could be adjusted using the fine-tunning function into a fixated-state in a frameless adaptor. We recommend that the navigation of the fixed-AR system should simultaneously utilize the frameless-fixation before pretreatment CBCT scanning. If a patient cannot endure the long beam-on time, a rest period should be included after frameless re-fixation is guided to the existing fixed-AR system. Frameless fixation can be conducted for a long time, which may result in pressure on the face and making the patient feel uncomfortable. For this reason, it is important to conduct the close initial position in frameless fixation.

This study has a few limitations. The fixed-AR system is not automatically registered to the object; it takes a few attempts to overlap the object and virtual models. The development of a fixed-AR system should be considered automatically to register into the object using real-time tracking, and we are planning to build a storage server with patient specific information, including virtual models in the fixed-AR application in order to conduct a clinical trial in the future. Although the virtual model of 3D-scanning consists of a fixed-AR system, it is still inaccurate to register it to the entire real object. 3D-scanning accuracy will determine the potential applications of 3D-scanners. There is still a limitation on scanning the entire object. Although 3D-scanning can guide the surface fixed-state, the general 3D-scanning accuracy of the entire object should be evaluated.

Conclusions

We demonstrated that fixed-AR is a useful tool for frameless fixation without CBCT at GKRS and installed software that included accurate mating to a 3D-printed patient model with flexible QR markers. This simple method using conventional equipment and fixed-AR with inside-out tracking could be directly adapted to GKRS. Overall, re-mask fixation guided by a fixed-AR system without CBCT scanning must be considered when planning for small lesions or eloquent areas. However, in cases of patients with large metastases, no eloquent area and continual movements under mask-fixation could be navigated well for repositioning using a fixed-AR system.

Declarations

Acknowledgments: This work was supported by the Korea Medical Device Development Fund granted by the Korean government (Ministry of Science and ICT, Ministry of Trade, Industry and Energy, Ministry of Health & Welfare, and Ministry of Food and Drug Safety) (Project Number: 202012E08).

Author contributions: Conception and design: HCM, YSD. Data acquisition: SJP, YDK. Data analysis and interpretation: KMK, HK, EJL, MSK, JWK, YHK. Manuscript preparation: HCM, CKP, YGK, YSD

Competing interests: Sang Joon Park is the founder and CEO of MEDICALIP. Chul-Kee Park and Yun-Sik Dho own stock options in MEDICALIP. Other authors have no conflict of interest to declare.

Data availability: The datasets used in this study are available from the corresponding author on reasonable request.

References

1. Breitbarth, A. *et al.* Measurement accuracy and dependence on external influences of the iPhone X TrueDepth sensor.*SPIE.***11144** (2019).
2. Camison, L. *et al.* Validation of the Vectra H1 portable three-dimensional photogrammetry system for facial imaging. *Int. J. Oral. Maxillofac. Surg*, **47**, 403–410 (2018).
3. Carminucci, A., Nie, K., Weiner, J., Hargreaves, E. & Danish, S. F. Assessment of motion error for frame-based and noninvasive mask-based fixation using the Leksell Gamma Knife Icon radiosurgery system. *J. Neurosurg*, **129**, 133–139 (2018).
4. Chung, H. T. *et al.* Assessment of image co-registration accuracy for frameless gamma knife surgery. *PLoS One*, **13**, e0193809 (2018).
5. Dho, Y. S. *et al.* Development of an inside-out augmented reality technique for neurosurgical navigation. *Neurosurg. Focus*, **51**, E21 (2021).

6. Duggar, W. N. *et al.* Gamma Knife((R)) icon CBCT offers improved localization workflow for frame-based treatment. *J. Appl. Clin. Med. Phys*, **20**, 95–103 (2019).
7. Hou, Y., Ma, L., Zhu, R., Chen, X. & Zhang, J. A low-cost iPhone-assisted augmented reality solution for the localization of intracranial lesions. *PLoS One*, **11**, e0159185 (2016).
8. Soeiro, J., Carmo, M. B. & Ferreira, H. A. Mobile solution for brain visualization using augmented and virtual reality. 20th International Conference Information Visualisation (IV):124–129(2016).
9. Kim, J. O. *et al.* Lunsford, L.D. Patient motion analysis of first 50 frameless fixation cases with Leksell Gamma Knife ICON. *IJROBP*, **102**, e495–e496 (2018).
10. Keisuke Hattori, T. H. Inside-out tracking controller for VR/AR HMD using image recognition with smartphones. SIGGRAPH '20: ACM SIGGRAPH 2020 Posters:1–2(2020).
11. Kim, H. Y. *et al.* Reliability of stereotactic coordinates of 1.5-Tesla and 3-Tesla MRI in radiosurgery and functional neurosurgery. *J. Korean Neurosurg. Soc*, **55**, 136–141 (2014).
12. Kim, J. W. *et al.* Fractionated stereotactic gamma knife radiosurgery for large brain metastases: a retrospective, single center study. *PLoS One*, **11**, e0163304 (2016).
13. Kockro, R. A. *et al.* Planning and simulation of neurosurgery in a virtual reality environment. *Neurosurgery*, **46**, 118–135 (2000).
14. Leksell, L. The stereotaxic method and radiosurgery of the brain. *Acta Chir. Scand*, **102**, 316–319 (1951).
15. Maciunas, R. J., Galloway, R. L. Jr. & Latimer, J. W. The application accuracy of stereotactic frames. *Neurosurgery*, **35**, 682–694 (1994).
16. Mohamed, S. A. S., Haghbayan, M., Westerlund, T., Heikkonen, J. & Tenhunen, H. Plosila, J. A survey on odometry for autonomous navigation systems. *IEEE Access*, **7**, 97466–97486 (2019).
17. Nermina Zaimovic-Uzunovic, S. L. Influences of surface parameters on laser 3D scanning. Imeko conference proceedings: international symposium on measurement and quality control(2010).
18. Park, H. R. *et al.* Frameless fractionated gamma knife radiosurgery with ICON for large metastatic brain tumors. *J. Korean Med. Sci*, **34**, e57 (2019).
19. Pavlica, M., Dawley, T., Goenka, A. & Schulder, M. Frame-based and mask-based stereotactic radiosurgery: the patient experience. *Compared. Stereotact. Funct. Neurosurg*, **99**, 241–249 (2021).
20. Qian Shan, T. E. D., Samavi, R. & Al-Rei, M. Augmented reality based brain tumor 3D visualization. *Procedia Comput. Sci*, **113**, 400–407 (2017).
21. Rava, P. *et al.* Feasibility and safety of cavity-directed stereotactic radiosurgery for brain metastases at a high-volume medical center. *Adv. Radiat. Oncol*, **1**, 141–147 (2016).
22. Sugiyama, T. *et al.* Immersive 3-dimensional virtual reality modeling for case-specific presurgical discussions in cerebrovascular neurosurgery. *Oper. Neurosurg*, **20**, 289–299 (2021).
23. Sun, G. C. *et al.* Impact of virtual and augmented reality based on intraoperative magnetic resonance imaging and functional neuronavigation in glioma surgery involving eloquent areas. *World Neurosurg*, **96**, 375–382 (2016).
24. Verdaasdonk, R. & Liberton, N. The Iphone X as 3D scanner for quantitative photography of faces for diagnosis and treatment follow-up (Conference Presentation). SPIE. 10869(2019).
25. Vogt, M., Rips, A. & Emmelmann, C. Comparison of iPad Pro®'s LiDAR and TrueDepth capabilities with an industrial 3D scanning solution. *Technologies*, **9**, 25 (2021).
26. Watanabe, E., Satoh, M., Konno, T., Hirai, M. & Yamaguchi, T. The trans-visible navigator: a see-through neuronavigation system using augmented reality. *World Neurosurg*, **87**, 399–405 (2016).

27. Wright, G., Schasfoort, J., Harrold, N., Hatfield, P. & Bownes, P. Intra-fraction motion gating during frameless Gamma Knife((R)) Icon therapy: the relationship between cone beam CT assessed intracranial anatomy displacement and infrared-tracked nose marker displacement. *J. Radiosurg. SBRT*, **6**, 67–76 (2019).
28. Yomo, S. & Hayashi, M. Is upfront stereotactic radiosurgery a rational treatment option for very elderly patients with brain metastases? A retrospective analysis of 106 consecutive patients age 80 years and older. *BMC Cancer*, **16**, 948 (2016).
29. Yoon, H., Kim, Y., Lim, Y. O. & Choi, K. Quality of life of older adults with cancer in Korea. *Soc. Work Health Care*, **57**, 526–547 (2018).
30. Zlatanova, D. D.I.S. Augmented Reality Technology in 2003.
31. Breitbarth, A. *et al. Measurement accuracy and dependence on external influences of the iPhone X TrueDepth sensor* Vol 11144 (SPIE, 2019).
32. Camison, L. *et al.* Validation of the Vectra H1 portable three-dimensional photogrammetry system for facial imaging. *Int J Oral Maxillofac Surg*, **47**, 403–410 (2018).
33. Carminucci, A., Nie, K., Weiner, J., Hargreaves, E. & Danish, S. F. Assessment of motion error for frame-based and noninvasive mask-based fixation using the Leksell Gamma Knife Icon radiosurgery system. *J Neurosurg*, **129**, 133–139 (2018).
34. Chung, H. T. *et al.* Assessment of image co-registration accuracy for frameless gamma knife surgery. *PLoS One*, **13**, e0193809 (2018).
35. Dho, Y. S. *et al.* Development of an inside-out augmented reality technique for neurosurgical navigation. *Neurosurg Focus*, **51**, E21 (2021).
36. Duggar, W. N. *et al.* Gamma Knife((R)) icon CBCT offers improved localization workflow for frame-based treatment. *J Appl Clin Med Phys*, **20**, 95–103 (2019).
37. Hou, Y., Ma, L., Zhu, R., Chen, X. & Zhang, J. A Low-Cost iPhone-Assisted Augmented Reality Solution for the Localization of Intracranial Lesions. *PLoS One*, **11**, e0159185 (2016).
38. Soeiro APC, J., Carmo, M. B. & Ferreira, H. A. Mobile Solution for Brain Visualization Using Augmented and Virtual Reality. 20th International Conference Information Visualisation (IV):124–129 2016
39. Kim, J. O., Bednarz, K. F. G., Huq, M. S. & Flickinger, J. C. Sr, E. Monaco ANaLDL: Patient Motion Analysis of First 50 Frameless Fixation Cases with Leksell Gamma Knife ICON.
40. International *Journal of Radiation Oncology*Biology*Physics*, **102**, e495–e496 (2018).
41. Keisuke Hattori, T. H. Inside-out Tracking Controller for VR/AR HMD using Image Recognition with Smartphones. SIGGRAPH '20: ACM SIGGRAPH 2020 Posters:1–2 2020
42. Kim, H. Y. *et al.* Reliability of Stereotactic Coordinates of 1.5-Tesla and 3-Tesla MRI in Radiosurgery and Functional Neurosurgery. *J Korean Neurosurg Soc*, **55**, 136–141 (2014).
43. Kim, J. W. *et al.* Fractionated Stereotactic Gamma Knife Radiosurgery for Large Brain Metastases: A Retrospective, Single Center Study. *PLoS One*, **11**, e0163304 (2016).
44. Kockro, R. A. *et al.* Planning and simulation of neurosurgery in a virtual reality environment. *Neurosurgery*, **46**, 118–135 discussion 135 – 117 (2000).
45. Leksell, L. The stereotaxic method and radiosurgery of the brain. *Acta Chir Scand*, **102**, 316–319 (1951).
46. Maciunas, R. J., Galloway, R. L. Jr. & Latimer, J. W. The application accuracy of stereotactic frames. *Neurosurgery*, **35**, 682–694 discussion 694 – 685 (1994).
47. Mohamed, S. A. S. *et al.* A Survey on Odometry for Autonomous Navigation Systems. *IEEE Access*, **7**, 97466–97486 (2019).

48. Nermina Zaimovic-Uzunovic, S. L. Influences of surface parameters on laser 3D scanning. IMEKO CONFERENCE PROCEEDINGS: INTERNATIONAL SYMPOSIUM ON MEASUREMENT AND QUALITY CONTROL 2010
49. Park, H. R. *et al.* Frameless Fractionated Gamma Knife Radiosurgery with ICON for Large Metastatic Brain Tumors. *J Korean Med Sci*, **34**, e57 (2019).
50. Pavlica, M., Dawley, T., Goenka, A. & Schulder, M. Frame-Based and Mask-Based Stereotactic Radiosurgery: The Patient Experience, Compared. *Stereotact Funct Neurosurg*, **99**, 241–249 (2021).
51. Qian Shan, T. E. D. & Reza Samavi Mona Al-Rei: Augmented Reality Based Brain Tumor 3D Visualization. *Procedia Computer Science*, **113**, 400–407 (2017).
52. Rava, P. *et al.* Feasibility and safety of cavity-directed stereotactic radiosurgery for brain metastases at a high-volume medical center. *Adv Radiat Oncol*, **1**, 141–147 (2016).
53. Sugiyama, T. *et al.* Immersive 3-Dimensional Virtual Reality Modeling for Case-Specific Presurgical Discussions in Cerebrovascular Neurosurgery. *Oper Neurosurg (Hagerstown)*, **20**, 289–299 (2021).
54. Sun, G. C. *et al.* Impact of Virtual and Augmented Reality Based on Intraoperative Magnetic Resonance Imaging and Functional Neuronavigation in Glioma Surgery Involving Eloquent Areas. *World Neurosurg*, **96**, 375–382 (2016).
55. Verdaasdonk, R. & Liberton, N. The Iphone X as 3D scanner for quantitative photography of faces for diagnosis and treatment follow-up (Conference Presentation): SPIE 2019, Vol 10869
56. Vogt, M., Rips, A. & Emmelmann, C. Comparison of iPad Pro®'s LiDAR and TrueDepth Capabilities with an Industrial 3D Scanning Solution. *Technologies*, **9**, 25 (2021).
57. Watanabe, E., Satoh, M., Konno, T., Hirai, M. & Yamaguchi, T. The Trans-Visible Navigator: A See-Through Neuronavigation System Using Augmented Reality. *World Neurosurg*, **87**, 399–405 (2016).
58. Wright, G., Schasfoort, J., Harrold, N., Hatfield, P. & Bownes, P. Intra-fraction motion gating during frameless Gamma Knife((R)) Icon therapy: The relationship between cone beam CT assessed intracranial anatomy displacement and infrared-tracked nose marker displacement. *J Radiosurg SBRT*, **6**, 67–76 (2019).
59. Yomo, S. & Hayashi, M. Is upfront stereotactic radiosurgery a rational treatment option for very elderly patients with brain metastases? A retrospective analysis of 106 consecutive patients age 80 years and older. *BMC Cancer*, **16**, 948 (2016).
60. Yoon, H., Kim, Y., Lim, Y. O. & Choi, K. Quality of life of older adults with cancer in Korea. *Soc Work Health Care*, **57**, 526–547 (2018).
61. Zlatanova, D. D. I. S. Augmented Reality Technology, in 2003

Figures

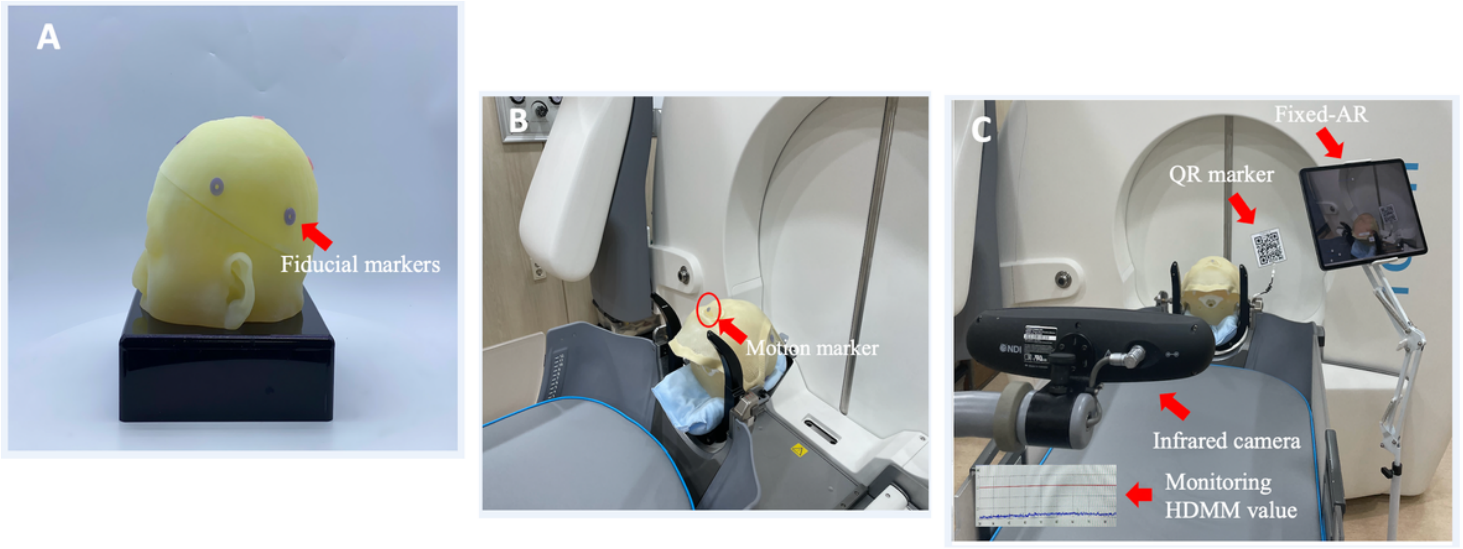

Figure 1

The virtual models and a 3D-printed model almost overlap using fixed-augmented reality. The virtual model based on 3D-scanning (A) and that based on cone-beam computed tomography (B) are shown.

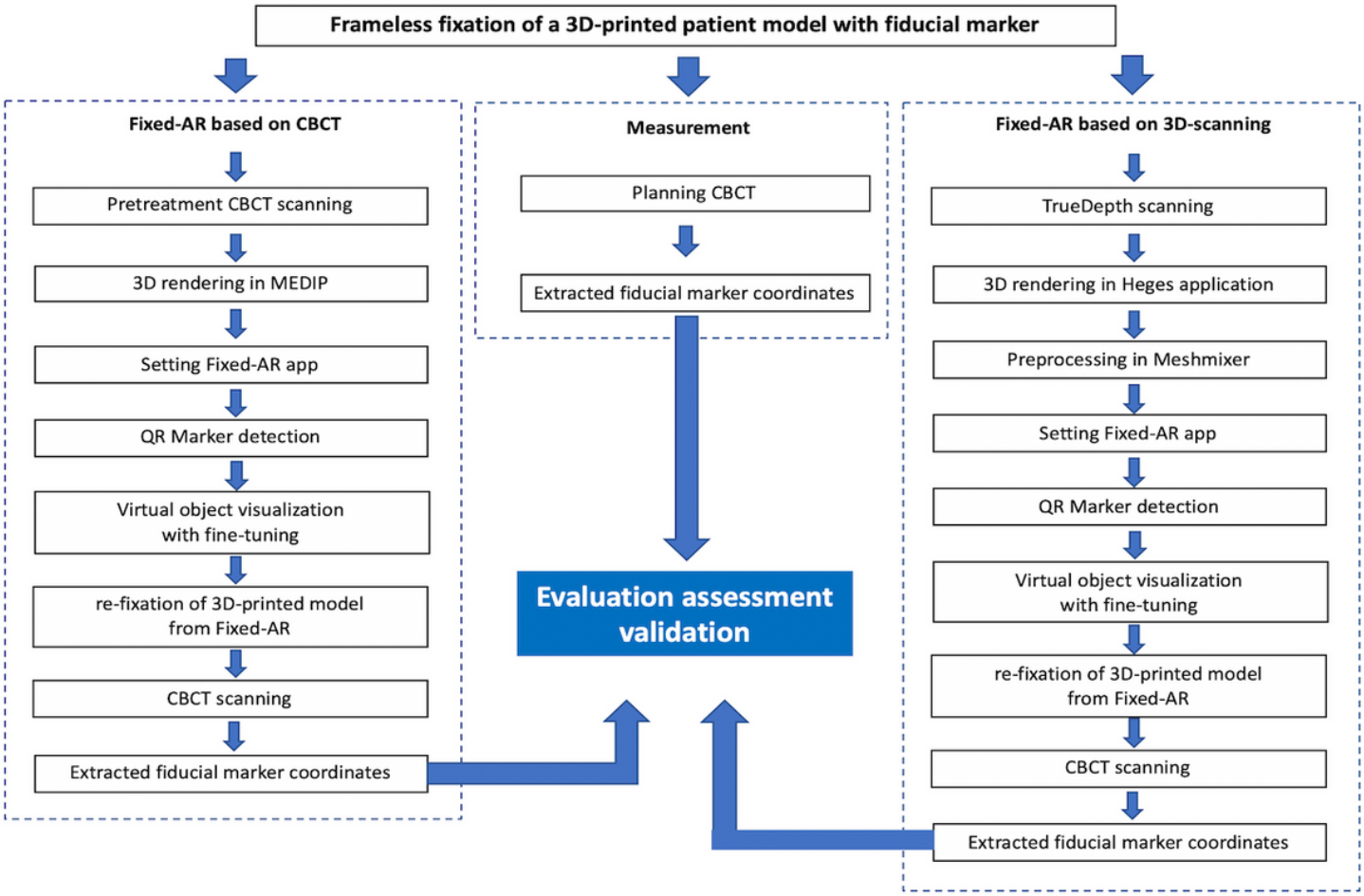

Figure 2

The fixed-AR execution prepared in the frameless fixation adaptor for gammaknife radiosurgery. The 3D-printed patient model included fiducial markers (A). The 3D-printed model had a frameless adaptor with the motion marker (B). Implemented fixed-AR with the QR marker being monitored under the infrared camera (C). Abbreviation: Quick Response, QR; Augmented Reality, AR; high-definition motion monitoring, HDMM.

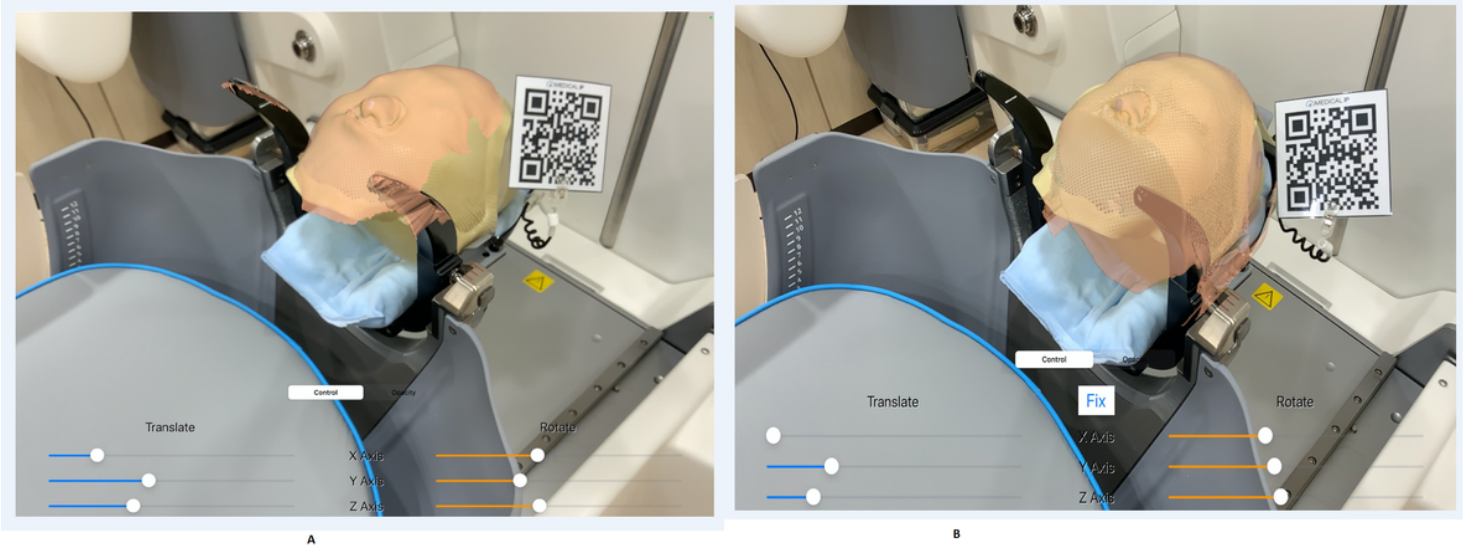

Figure 3

Schematic illustration of the procedure to evaluate frameless fixation for gammaknife radiosurgery